Liquid phase stabilization versus bubble formation at a nanoscale curved interface

Jarrod Schiffbauer[1,*] and Tengfei Luo[2,3,†]

[1]*Colorado Mesa University, Department of Physical and Environmental Sciences, Grand Junction, Colorado 81503, USA*

[2]*University of Notre Dame, Department of Aerospace and Mechanical Engineering, Notre Dame, Indiana 46556, USA*

[3]*Center for Sustainable Energy at Notre Dame, Notre Dame, Indiana 46556, USA*

(Received 5 November 2016; revised manuscript received 21 June 2017; published 19 March 2018)

We investigate the nature of vapor bubble formation near a nanoscale-curved convex liquid-solid interface using two models: an equilibrium Gibbs model for homogenous nucleation, and a nonequilibrium dynamic van der Waals–diffuse-interface model for phase change in an initially cool liquid. Vapor bubble formation is shown to occur for sufficiently large radius of curvature and is suppressed for smaller radii. Solid-fluid interactions are accounted for and it is shown that liquid-vapor interfacial energy, and hence Laplace pressure, has limited influence over bubble formation. The dominant factor is the energetic cost of creating the solid-vapor interface from the existing solid-liquid interface, as demonstrated via both equilibrium and nonequilibrium arguments.

DOI: 10.1103/PhysRevE.97.033106

I. INTRODUCTION

A number of potentially transformative technologies rely on energy and momentum transfer between a hot, nanostructured solid and a surrounding fluid [1,2]. These span applications as diverse as plasmonic photothermal cancer therapy [3–6], photocatalysis [7,8], solar-powered water desalination [9–12], and physicochemical separations [13]. Metallic [14,15], metal-dielectric structured [16], and/or molecularly functionalized nanoparticles (NPs) [17,18] have been studied as candidates for many of these applications. Nanoscale cavitation-oscillation [19–23] and phase-change phenomena [24] have been reported, but a simple thermodynamic criterion for vapor bubble formation, analogous to nanocrystal nucleation in a melt [25] (or cavitation from a *bulk* fluid), is conspicuously lacking. While it is known that interfacial forces and molecular structure affects heat transport [26,27], the roles of interfacial energies, viscous dissipation, and phase change near nanoscale interfaces [24,28–30] remain somewhat unclear.

Nanoscale-confined phase stabilization due to surface-fluid interaction has been predicted under a variety of circumstances (see [28,29] for example). However, the phase stability of a liquid layer surrounding small gold nanoparticles observed in molecular dynamics simulations [24,30] is quite curious; it is not *a priori* clear how the curvature of a convex solid-fluid interface would stabilize the heated fluid against vaporization. One hypothesis is that the Laplace pressure required to sustain a stable bubble of small radius is too high and this suppresses vapor formation at the interface [24]. Here we examine the issue by considering both equilibrium vapor formation criteria and nonequilibrium hydrodynamic calculations. However, we frame the discussion in terms of interfacial energies, rather than Laplace pressure [25].

II. EQUILIBRIUM THERMODYNAMICS

To gain some intuition into the roles of geometry via surface forces, we first consider the equilibrium nucleation of a vapor layer of thickness $\delta\tilde{r}$ [31] from a liquid at uniform temperature $\tilde{T}$ surrounding a particle of radius $\tilde{r}$ (see Fig. 1). We follow a similar line of thinking employed to understand the thermodynamics of nanoparticle nucleation in a melt [25]. The change in Gibbs free energy is the (reversible) free energy change associated with an input heat of $\tilde{T}\Delta\tilde{S}_{\mathrm{LV}}$ turning liquid near an existing solid-liquid interface into a vapor layer with a solid-vapor and a liquid-vapor interface. By considering the difference in Gibbs energy per mole between the final state of thin vapor layer + bulk liquid + solid-vapor + liquid-vapor interfaces and the initial state of bulk liquid + solid-liquid interface, then multiplying by the number of moles of vapor contained in a thin spherical shell of thickness $\delta\tilde{r}$, one obtains

$$\begin{aligned}\Delta\tilde{G}_{\mathrm{total}} = {} & \frac{4\pi}{3}\frac{(\Delta\tilde{H}_{\mathrm{LV}} - \tilde{T}\Delta\tilde{S}_{\mathrm{LV}})(\tilde{R}^3 - \tilde{r}^3)}{\tilde{V}_V} \\ & + 4\pi\left[\frac{\gamma_{\mathrm{SV}}(\tilde{R}^3 - \tilde{r}^3)}{\tilde{r}} + \frac{\gamma_{\mathrm{LV}}(\tilde{R}^3 - \tilde{r}^3)}{\tilde{R}}\frac{\tilde{V}_L}{\tilde{V}_V}\right. \\ & \left. - \frac{\gamma_{\mathrm{SL}}(\tilde{R}^3 - \tilde{r}^3)}{\tilde{r}}\frac{\tilde{V}_L}{\tilde{V}_V}\right]. \end{aligned} \tag{1}$$

Here, $\tilde{R} = \tilde{r} + \delta\tilde{r}$, and the phase (solid, liquid, vapor) for the molar volumes $\tilde{V}$ changes in enthalpy $\tilde{H}$ and entropy $\tilde{S}$, as well as interfacial tensions γ, are denoted by respective subscripts S, L, and V. Minimizing Eq. (1) with respect to radius $\tilde{r}$, keeping terms to leading order in $\delta\tilde{r}$, and using Young's equation, $\gamma_{\mathrm{SV}} = \gamma_{\mathrm{LV}}\cos\theta + \gamma_{\mathrm{SL}}$, yields a critical particle radius for formation of a thin vapor layer ($\delta\tilde{r} \ll \tilde{r}$),

$$\tilde{r}_{\mathrm{cr}} = \frac{\gamma_{\mathrm{LV}}(5\tilde{V}_V\cos\theta + 3\tilde{V}_L) + 5\gamma_{\mathrm{SL}}\Delta\tilde{V}_{\mathrm{LV}}}{-2(\tilde{T}\Delta\tilde{S}_{\mathrm{LV}} - \Delta\tilde{H}_{\mathrm{LV}})}. \tag{2}$$

Consider Eq. (1) with $\gamma_{\mathrm{LV}} = 3.4$ mN/m (argon) for a range of contact angles (with respect to the flat equilibrium interface)

*jschiffb@nd.edu

†Corresponding author: tluo@nd.edu

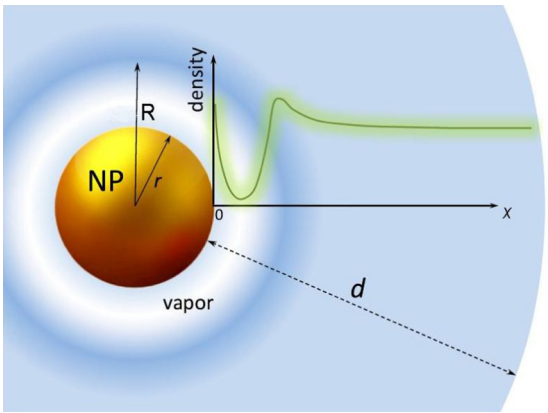

FIG. 1. Schematic of coordinates for system showing inner surface at r, vapor bubble between r and R, and the bulklike liquid. Note that d is chosen to be large enough that any pressure waves reflected from the outer boundary, where the pressure is held constant, do not have sufficient time to return to the bubble region during the course of simulation.

and ratios of γ_{SL}/γ_{LV} (see Fig. 2). Increasing the solid-fluid surface energy corresponds to a higher barrier-to-vapor formation for radii below $\Delta\tilde{G}_{\text{total}} = 0$ and greater release of energy above. Similarly, hydrophilic surfaces, $\theta < \pi/2$, have a higher barrier to vapor-layer formation than hydrophobic surfaces, $\theta > \pi/2$, and result in a smaller release of energy for spontaneous transition.

Comparing the mercury-liquid interfaces for several liquids with various liquid-vapor interfaces [32], the solid-vapor and solid-liquid interfacial energies for fluid-metal interfaces can be estimated to be about an order of magnitude larger than typical liquid-vapor interfacial energies. Below the critical temperature T_c, the ratio of molar volumes will be < 1; for example, argon has ratios ranging from 10^{-3}–10^{-1} up to about $T = 0.85T_c$ (128 K) [33]. So the solid-liquid and liquid-vapor contributions to Eq. (1) are generally smaller than the solid-vapor contribution. The critical radius (inset,

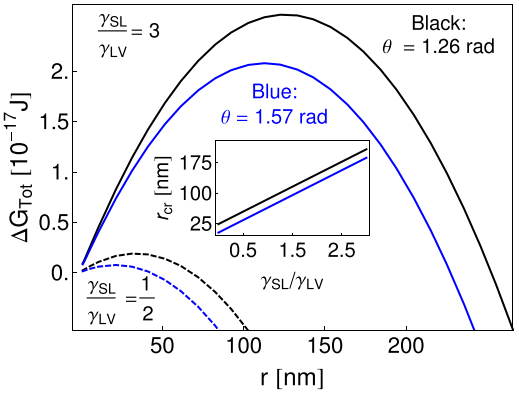

FIG. 2. The Gibbs free energy change, Eq. (1), at $T = 0.85T_c$ for argon on a goldlike nanosphere for $\delta r = 1$ nm, for hydrophilic ($\theta = 1.26$ rad) and hydrophobic ($\theta = 1.57$ rad) surfaces with different strengths of solid-fluid interaction, as determined by γ_{SL}/γ_{LV}. (Inset) The critical radius estimates for the same angles as a function of γ_{SL}/γ_{LV}.

Fig. 2) increases with increasing solid-vapor interfacial energy. Even in the limit of vanishing liquid-vapor interfacial tension, a nonzero solid-vapor interfacial energy can inhibit vapor formation. Thus the dominant factor in vapor formation is not the liquid-vapor interfacial energy, in agreement with [34], but rather the energetic cost of creating the solid-vapor interface.

The energetic criterion for reversible formation of a vapor layer in a uniformly heated liquid is given by Eq. (1). However, an initially cold liquid in contact with a hot particle will undergo heating, expansion, and phase change. Viscous dissipation has been shown to play an important role in nonequilibrium bubble dynamics [35], so the Gibbs approach can provide a lower bounds for the energy required to nucleate a bubble. But a nonequilibrium theory is required to shed light on the dynamics of vaporization in an initially cool liquid placed in contact with a hot solid.

III. NONEQUILIBRIUM THERMODYNAMICS

Because the diffuse-interface–dynamic van der Waals theory [36–43] has been used previously to study bubble dynamics [23,35], in good agreement with the classical Rayleigh-Plesset equation, molecular dynamic (MD) simulations [21], and experiments [19] of bubble growth and collapse, we adopt a variation on this model. We wish to isolate the roles of viscous dissipation, capillary forces, and interfacial curvature on the phase change and heat transfer properties of the fluid from considerations of energy transport and capacity of the solid. Therefore we consider the evolution of an initially uniform fluid held between rigid, impenetrable surfaces of infinite interfacial conductance (see Fig. 1) in thermal equilibrium with infinite capacity baths at fixed temperatures $T(r) = 0.85T_c$ and $T(r + d) = 0.56T_c$.

The model is formulated using hydrodynamic conservation equations for mass, momentum, and energy [40–42] supplemented by appropriate boundary conditions. The (dimensional) governing equations are as follows, with the '˜' denoting dimensional variables: Continuity,

$$\partial_t \tilde{n} + \nabla \cdot (\tilde{n}\tilde{\mathbf{v}}) = 0, \tag{3}$$

where $\tilde{n}$ is the number density. The fluid velocity $\tilde{\mathbf{v}}$ is given by

$$M\tilde{n}(\partial_t \tilde{\mathbf{v}} + \tilde{\mathbf{v}} \cdot \nabla\tilde{\mathbf{v}}) = -\nabla \cdot (\tilde{\mathbb{P}} - \tilde{\mathbb{D}}), \tag{4}$$

with molecular mass M, pressure, and viscous dissipation tensors $\tilde{\mathbb{P}}$ and $\tilde{\mathbb{D}}$, respectively. The temperature is governed by

$$\tilde{c}_v(\partial_t \tilde{T} + \tilde{\mathbf{v}} \cdot \nabla\tilde{T}) = -\tilde{\ell}\nabla \cdot \tilde{\mathbf{v}} + \nabla(\lambda\nabla\tilde{T}) + \tilde{\mathbb{D}} : \nabla\tilde{\mathbf{v}}, \tag{5}$$

with thermal conductivity λ and the Clapeyron coefficient defined $\tilde{\ell} = \tilde{T}(\partial\tilde{P}_{\text{bulk}}/\partial\tilde{T})_n$. Elementwise, the dissipation tensor is

$$\tilde{D}_{i,j} = \eta\left(\partial_i\tilde{v}_j + \partial_j\tilde{v}_i - \tfrac{2}{3}\nabla \cdot \tilde{\mathbf{v}}\hat{\delta}_{i,j}\right) + \mu\nabla \cdot \tilde{\mathbf{v}}\hat{\delta}_{i,j}, \tag{6}$$

where η and μ are the shear and bulk viscosities, and $\hat{\delta}_{i,j}$ is the Kronecker δ.

The one-density van der Waals theory includes a density gradient contribution to the free energy density [38,42,43]. Thus pressure tensor elements are defined with a gradient contribution as $\tilde{P}_{i,j} = [\tilde{n}k_B\tilde{T}/(1 - \Omega_o\tilde{n}) - \varepsilon\Omega_o\tilde{n}^2 - C\tilde{T}\tilde{n}\nabla^2\tilde{n} + C\tilde{T}(\nabla\tilde{n})^2]\hat{\delta}_{i,j} + C\tilde{T}\partial_i\tilde{n}\partial_j\tilde{n}$, where Ω_o

and ε are the Lennard-Jones (L-J) volume and well depth, respectively, k_B is the Boltzmann constant, and C is the density gradient coupling parameter, which we discuss subsequently.

Rather than using the full three-dimensional formulation, we neglect angular nonuniformity in surface temperature and restrict ourselves to cases with radial symmetry. The divergence operator is then written $\mathcal{D}_m[\varphi(x)] = x^{-m}\partial_x[x^m\varphi(x)]$, with $m = 0$ representing planar and $m = 2$ spherical symmetry. The specific heat is written $\tilde{c}_V = 3k_B\tilde{n}/2$, and the Clapeyron coefficient is obtained from the bulk (dimensionless) pressure $P = nT/(1-\alpha n) - \frac{27}{8}\alpha n^2$. We further assume $\eta \approx \mu = \nu M\tilde{n}$ with a constant kinematic viscosity ν for simplicity. This also permits control of viscous dissipation in a convenient way. The thermal conductivity is taken to be $\lambda = k_B\nu\tilde{n}$, following [43].

This permits the reduction of the full model, Eqs. (3)–(5), to a set of dimensionless, one-dimensional (1D) governing equations:

$$\partial_t n + \mathcal{D}_m[nv] = 0 \tag{7}$$

and

$$n\partial_t v + nv\partial_x v = \mathcal{D}_m[D_{xx} - P_{xx}], \tag{8}$$

where

$$D_{xx} - P_{xx} = \frac{9}{8}\alpha n^2 - \frac{1}{3}\frac{nT}{1-\alpha n} + \delta nT\left(\frac{m\partial_x n}{x} + \partial^2_{xx} n\right) - \frac{3}{2}\delta T(\partial_x n)^2 + \frac{7}{3}\beta n\partial_x v + \frac{1}{3}\frac{m\beta nv}{x} \tag{9}$$

and the temperature profile is given by

$$\frac{3}{2}n\partial_t T = \mathcal{D}_m[\beta n\partial_x T] - \frac{nT}{1-\alpha n}\mathcal{D}_m[v] - \frac{3}{2}nv\partial_x T + \frac{7}{9}\beta n(\partial_x v)^2 + \frac{1}{9}\frac{m\beta nv\partial_x v}{x}. \tag{10}$$

The L-J parameters for argon, $\varepsilon = 7.033\times10^{-21}$ J and $\Omega_o^{1/3} = 0.345$ nm, set the energy and length scales. The number density is scaled by the liquid bulk number density n_{LB} at pressure 100 kPa and temperature $T = 0.56T_c$, where T_c normalizes the temperature. Velocity and time scales may then be defined $v_o = \sqrt{3k_BT_c/M} = 97$ m/s and $\tau_o = \Omega_o^{1/3}/v_o = 3.5$ ps. Assuming a constant kinematic viscosity ν, three dimensionless parameters describe the dynamics: the excluded volume fraction $\alpha = \Omega_o n_{\mathrm{LB}}$, an inverse Reynolds number $\beta = \nu/\Omega_o^{1/3}v_o$ controlling viscous dissipation and thermal conductivity, and a capillarity parameter $\delta = Cn_{\mathrm{LB}}/3k_B\Omega_o^{2/3}$.

The gradient coupling parameter C is related to the equilibrium liquid-vapor surface tension through the action integral over the density [38,44], assuming C is a constant [23,35,43]. Note, however, for typical substances [33], the values of C thus obtained vary by over an order of magnitude with temperature. While n, P, and T are held constant at the exterior (cold) boundary, the interior boundary condition, $\partial_x n|_{x=r} = -\chi/T(r)$, accounts for adsorption at the solid surface where $\chi = \phi_o\Omega_o^{1/3}/CT_cn_{\mathrm{LB}}$ with wetting potential ϕ_o [35,43]. ϕ_o can be related to the contact angle for the appropriate liquid-vapor-solid equilibrium for a flat interface [35], again assuming independence of state. For simplicity, we treat β, δ, and χ as free parameters with a range informed by data for argon [33]. A more physically realistic model would include a state-dependent viscosity (see for instance [23]). But for a constant capillary coupling across the range of physically reasonable values for viscosity [33], bulklike energy and momentum transport will dominate the leading-order dynamics over capillary forces.

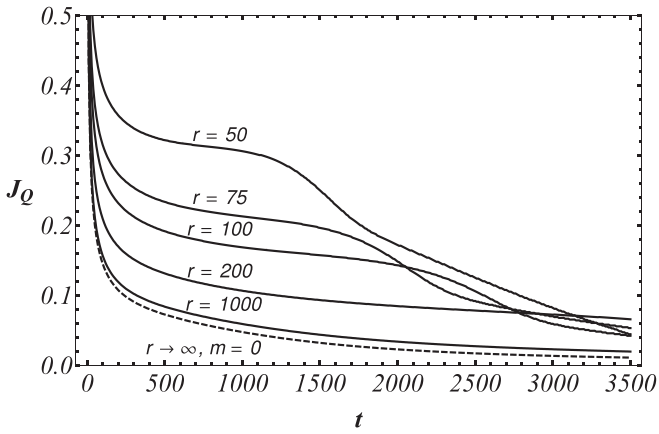

FIG. 3. Heat flux into hot boundary for varying inner radius r_{np}. The calculation uses a fixed kinematic viscosity 1.67×10^{-6} m^2/s, with $\alpha = 0.208$, $\beta = 47.192$, $\delta = 10^{-3}$, and $\chi = -10^{-3}$.

To simulate evolution of an initially uniform fluid of temperature $T = 0.56$ and density $n = 1.005$ in contact with a nanocurved surface of infinite heat capacity and infinite interfacial conductance (see Fig. 1 main text), the governing equations are solved numerically on a 1D grid for several values of boundary radius r with $m = 0,2$. The boundary conditions are $T(r,t) = 0.85$ and $T(d+r,t) = 0.56$, $P(x,0) = P(d+r,t) = 0.0059$ (about 0.7 MPa), $n(d+r,t) = 1.005$, $v = 0$ at both interfaces.

For preliminary runs, we choose parameters from the lower end of the range, $\delta = 10^{-9}$ and $\delta = 10^{-3}$, and $\chi = -10^{-3}$ (weakly hydrophilic surface with low capillary contribution). The input heat flux, $-\beta n\partial_x T(x = r)$, is evaluated as an average over the first few grid points and plotted in Fig. 3. However, numerical solutions were obtained for a range of parameters, $\delta \approx 10^{-9}$–10^{-1}, $\|\chi\| \approx -10^{-3}$–10, and $\beta \approx$ 10–10^2. We present results illustrating the general conclusions, as well as a few interesting cases. Overall, the heat flux into interfaces with smaller radii is higher, as might be expected from purely geometric effects, and the heat flux response with increasing radius is seen to approach the planar $m = 0$ case in the limit $r \to \infty$.

Here we summarize and discuss the main results and compare them to the Gibbs model. Density profiles $n(x,t)$ are shown in Fig. 4 for several different inner radii r at $t = 3500$ for $\delta = 10^{-3}$ and weakly hydrophilic surface, $\chi = 10^{-3}$. The density for $r = 50$ (about $\tilde{r} = 18$ nm) does not exhibit vapor formation. Instead, a layer of high-density liquid forms adjacent to the heated surface. For larger radii (between $150 \leqslant r \leqslant 200$), a liquid-vapor interface begins to develop. As r increases, the spherical $m = 2$ model approaches planar $m = 0$ behavior. The model predictions are within a reasonable

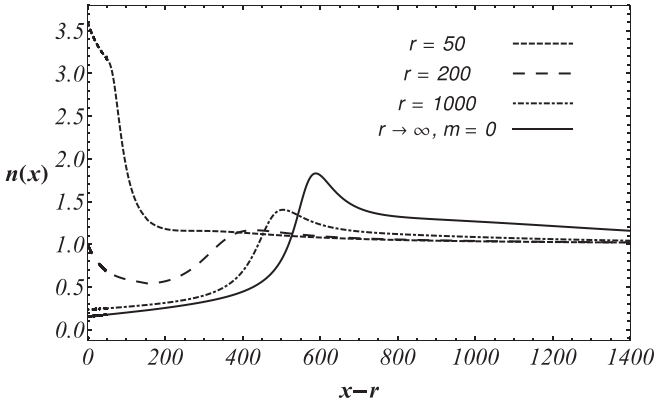

FIG. 4. Density profile at $t = 3500$ vs x, the radial distance from the particle surface see also (1) for several different inner radii r showing liquid phase stabilization at small radius and bubble formation and expansion at large radius, converging to the planar case as $r \to \infty$. The viscosity is $\nu = 1.67 \times 10^{-6}$ m^2/s and $\alpha = 0.208$, $\beta = 47.192$, $\delta = 10^{-3}$, and $\chi = -10^{-3}$, a weakly hydrophilic surface.

range of Gibbs radius for argon with weak surface-liquid forces (see Fig. 2 inset.)

Since $\delta \approx O(\gamma_{LV}^2)$, the range $\delta = 10^{-9}$–10^{-1} corresponds to a range of 4 orders of magnitude in equilibrium liquid-vapor energy. Physically reasonable values for argon are at the upper end of this range. Changing δ alone has no appreciable effect on vapor layer formation. However, modest change in β has a pronounced effect (Fig. 5). This is unsurprising. The capillary terms in Eq. (9) give higher-order contributions to the dynamics. In the present model, nonequilibrium phase stabilization originates in the x^{-1} radial contribution to the viscous dissipation and thermal conductivity, represented by the last terms in each of Eqs. (9) and (10), respectively. In the limit $r \to \infty$, the radial component of the dissipation vanishes and a vapor layer forms regardless of β.

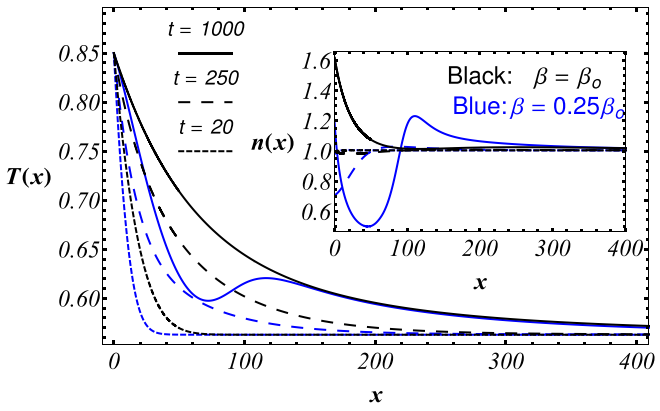

FIG. 5. Several snapshots of the temperature profiles for $\beta_o = 47.192$ and $0.25\beta_o$, and $\chi = -10^{-3}$. Inset shows a comparison of the density profiles near the interface for $t = 1000$. Calculations for a range of $\delta = 10^{-9}$–10^{-1} show essentially the same behavior.

IV. DISCUSSION AND CONCLUSIONS

Though we cannot directly compare the equilibrium Gibbs formulation and the nonequilibrium formulation, we may use the former to gain some deeper insight into the latter. For larger β and/or smaller r, heat conduction near the interface is rapid, resulting in a broader temperature distribution, and dissipative losses are high (Fig. 5). According to the Gibbs formulation in Eq. (1), the magnitude of the free energy change required for layer formation at a subequilibrium radius increases with increasing thickness $\delta\tilde{r}$ of the hot layer. This suggests, despite the local temperature, the fluid close to the interface cannot accumulate enough internal energy to undergo phase change. The liquid-vapor interfacial tension, via realistic values of the capillary parameter, however, appears to have little effect on the dynamics of the model, whereas the viscosity and thermal conductivity, which give rise to dissipative dynamics, obviously do not appear in the Gibbs formulation. Nonetheless, the picture which emerges from the nonequilibrium calculations is consistent with the equilibrium criterion inasmuch as the dissipative terms compete with the creation of the solid-vapor interface.

Following Lombard *et al.* [35], the solid-fluid forces are parameterized by the contact angle, yielding a wetting potential ϕ_o [43]. The model does not predict a phase stabilization effect based on the variation of χ alone, and vapor-layer formation was affected primarily by β and r. The wettability, parameterized by χ, influences interfacial heat transfer via the establishment of short-range density gradients (see Fig. 6), increasing or decreasing local conductivity. Hydrophilic surface interactions show enhancement over neutral interfaces, while hydrophobic interfaces result in reduced heat transport, in qualitative agreement with analytic [45] and molecular-dynamics [27,46] results.

There is some question regarding the ability of a continuum model to capture the physics of a fully-developed liquid-vapor interface of thickness approaching molecular dimensions [47]. But this is not critical for initial vapor formation and early dynamics. The gradients $\partial_x n$ are initially small and the dissipation terms are dominant over capillary forces, since physically realistic $\delta < \beta$ by roughly 2 orders of magnitude across the temperature range [33]. Regarding surface forces, despite qualitative agreement with other results, the present treatment seems inadequate. Estimating the range of surface forces by the extent of hydrophobic and hydrophilic boundary layers, there is no influence beyond about the L-J minimum, $2^{1/6}\Omega_o^{1/3}$. This is consistent with the repulsive component of a typical surface force, but the range of attractive forces is larger. Moreover, a continuous gradient cannot exist on a molecular length scale, except as an average over fluctuations. Lastly, the relationship between θ and ϕ_o [35] is based on the three-phase equilibrium [38,44] but includes only two of the four equilibrium parameters appearing in Young's equation.

The liquid density near the interface in the $r = 50$ case (see Fig. 4) is high compared to atomistic simulations [24,30] and the apparent minimum radius about an order of magnitude larger than determined by MD [30]. But the two pictures agree qualitatively; there is a particle radius below which a superheated liquid layer remains at the interface and the

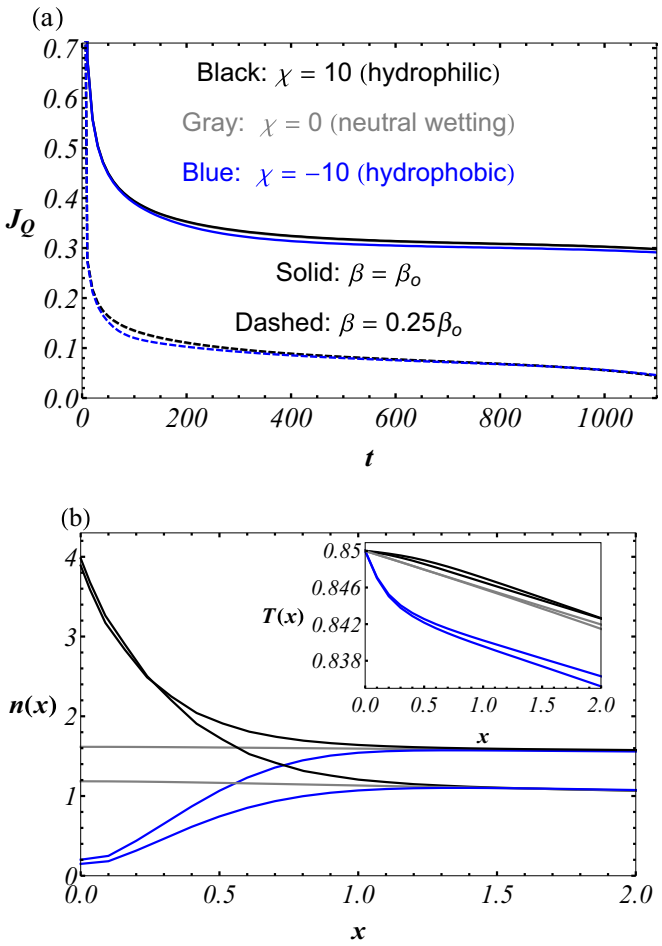

FIG. 6. Heat flux (top) and interfacial density profiles (bottom) for strongly hydrophilic, $\chi = 10$, strongly hydrophobic, $\chi = -10$, and neutral, $\chi = 0$, interfaces. Inset shows a comparison of the density profiles near the interface for $t = 1000$. Calculations are shown for $\delta = 10^{-2}$. The surface interaction enters in the capillary terms and is much weaker for small δ.

liquid-vapor interface does not form. The discrepancies are attributed to surface-fluid interactions, as well as variation in viscosity with temperature. Interestingly, a number of experimental [48] and first-principles simulations [49,50] show modulation of the effective solvent viscosity and mass transport near nanoscale solid-fluid interfaces. While the correspondence between the solid-fluid and the liquid-vapor interfacial contribution to the Gibbs energy is clear, the nonequilibrium model makes no distinction, except through viscosity, thermal conductivity, and density. Two important aims of ongoing work motivated by these results are to clarify the relationship between viscosity and thermal conductivity and to better understand the influence of surface-fluid forces via the inclusion of a body-force term in comparison to molecular simulations.

In conclusion, both equilibrium and nonequilibrium arguments demonstrate the critical factor in bubble formation is the cost of creating the solid-vapor interface, rather than the energetic cost of liquid-vapor interfacial formation. Furthermore, it was demonstrated that rapid heat conduction and viscous dissipation near the curved interface can prevent bubble formation. The relationship between viscous dissipation and interfacial forces is of fundamental and practical interest for nanoscale systems, where fluctuations and molecular structure play important roles near interfaces, yet a continuum theory still captures the essential dynamics of the overall system.

The results suggest that one can optimize nanoscale solid-fluid heat transfer and control nanoscale boiling by tailoring both geometry and surface properties, which affect the structure, and hence viscosity, of adjacent fluid layers [27]. The Gibbs criterion predictions regarding heat and momentum transfer at hydrophobic vs hydrophilic nanocurved surfaces can be tested. This would not only be of fundamental interest, but regarding applications such as cancer plasmonic photothermal therapy (PPT), solar desalination, or separations, controlling particle interfacial thermal and momentum transport through a combination of particle size and surface properties is of great practical value.

ACKNOWLEDGMENTS

We gratefully acknowledge ND Energy for support through the ND Energy Postdoctoral Fellowship program and the Army Research Office, Grant No. W911NF-16-1-0267, managed by Dr. Chakrapani Venanasi. National Science Foundation (1706039) and Center For the Advancement of Science in Space (CASIS, GA-2018-268)

[1] M. Hu and G. Hartland, J. Phys. Chem. B **106**, 7029 (2002).
[2] S. Boriskina, H. Ghasemi, and G. Chen, Mater. Today **16**, 375 (2013).
[3] X. Huang, P. Jain, I. El-Sayed, and M. El-Sayed, Lasers Med. Sci. **23**, 217 (2008).
[4] D. Lapotko, Cancers **3**, 802 (2011).
[5] L. Kennedy, L. Bickford, N. Lewinski, A. Coughlin, Y. Hu, E. Day, J. West, and R. Drezek, Small **7**, 169 (2011).
[6] Z. Qin and J. Bischof, Chem. Soc. Rev. **41**, 1191 (2012).
[7] A. Khanna and V. Shetty, Solar Energy **99**, 67 (2014).
[8] H. Liu, M. Li, T. Dao, Y. Liu, W. Zhou, L. Liu, X. Meng, T. Nagao, and J. Ye, Nano Energy **26**, 398 (2016).
[9] A. Polman, ACS NANO **7**, 15 (2013).
[10] O. Neumann, A. Urban, J. Day, S. Lal, P. Nordlander, and N. Halas, ACS Nano **7**, 42 (2013).
[11] L. Sahota and G. Tiwari, Solar Energy **130**, 260 (2016).
[12] L. Zhou, Y. Tan, J. Wang, W. Xu, Y. Yuan, W. Cai, S. Zhu, and J. Zhu, Nat. Photonics **10**, 393 (2016).
[13] O. Neumann, A. Neumann, E. Silva, C. Ayala-Orozco, S. Tian, P. Nordlander, and N. Halas, ACS NanoLett **15**, 7880 (2015).
[14] O. M. Wilson, X. Hu, D. G. Cahill, and P. V. Braun, Phys. Rev. B **66**, 224301 (2002).
[15] M. Hu, H. Petrova, and G. Hartland, Chem. Phys. Lett. **391**, 220 (2004).
[16] M. Hu, X. Wang, G. Hartland, V. Salgueirino-Maciera, and L. Liz-Marzan, Chem. Phys. Lett. **372**, 767 (2003).

[17] H. Patel, S. Das, T. Sundararajan, S. Nair, B. George, and T. Pradeep, Appl. Phys. Lett. **83**, 2931 (2003).
[18] K. Stocker, S. Neidhard, and J. Gezelter, J. Appl. Phys. **119**, 025106 (2016).
[19] V. Kotaidis and A. Plech, Appl. Phys. Lett. **87**, 213102 (2005).
[20] E. Lukianova-Hleb, Y. Hu, L. Latterini, L. Tarpani, S. Lee, R. Drezek, J. Hafner, and D. Lapotko, ACS Nano **4**, 2109 (2010).
[21] K. Sasikumar and P. Keblinski, J. Chem. Phys. **141**, 234508 (2014).
[22] L. Hou, M. Yorulmaz, N. Verhart, and M. Orrit, New J. Phys **17**, 013050 (2015).
[23] J. Lombard, T. Biben, and S. Merabia, Phys. Rev. Lett. **112**, 105701 (2014).
[24] S. Merabia, P. Keblinski, L. Joly, L. J. Lewis, and J.-L. Barrat, Phys. Rev. E. **79**, 021404 (2009).
[25] G. Kaptay, J. Nanosci. Nanotechnol. **12**, 2625 (2012).
[26] F. Sun, T. Zhang, M. Jobbins, Z. Guo, Z. Zheng, D. Tang, S. Ptaskinska, and T. Luo, Adv. Mater. **26**, 6093 (2014).
[27] B. Ramos-Alvarado, S. Kumar, and G. Peterson, J. Phys. Chem. Lett. **7**, 3497 (2016).
[28] R. Evans and P. Tarazona, Phys. Rev. Lett. **52**, 557 (1984).
[29] K. Binder, D. P. Landau, and A. M. Ferrenberg, Phys. Rev. Lett. **74**, 298 (1995).
[30] K. Sasikumar, Z. Liang, D. Cahill, and P. Keblinski, J. Chem. Phys. **140**, 234506 (2014).
[31] A ‘˜’ is used to denote dimensional variables. Nondimensional variables, as well as constants, are left unadorned.
[32] A. Adamson and A. Gast, *Physical Chemistry of Surfaces* (Wiley-Interscience, New York, 1997).
[33] *Thermophysical Properties of Fluid Systems*, accessed: 2016-09-30, URL http://webbook.nist.gov/chemistry/fluid/.
[34] J. Lombard, T. Biben, and S. Merabia, J. Phys. Chem. C **121**, 15402 (2017).
[35] J. Lombard, T. Biben, and S. Merabia, Phys. Rev. E **91**, 043007 (2015).
[36] P. Hohenberg and B. Halperin, Rev. Mod. Phys. **49**, 435 (1977).
[37] L. A. Turski and J. S. Langer, Phys. Rev. A **22**, 2189 (1980).
[38] J. Rowlinson and B. Widom, *Molecular Theory of Capillarity* (Oxford University Press, Oxford, UK, 1982).
[39] D. M. Anderson and G. B. McFadden (unpublished).
[40] V. Babin and R. Holyst, J. Chem. Phys **122**, 024713 (2005).
[41] V. Babin and R. Holyst, J. Phys. Chem. B **109**, 11367 (2005).
[42] A. Onuki, Phys. Rev. E **75**, 036304 (2007).
[43] R. Teshigawara and A. Onuki, Phys. Rev. E **82**, 021603 (2010).
[44] P. deGennes, Rev. Mod. Phys. **57**, 827 (1985).
[45] M. Caplan, A. Giri, and P. Hopkins, J. Chem. Phys. **140**, 154701 (2014).
[46] A. Tascini, J. Armstrong, E. Chiavazzo, M. Fascano, P. Asinari, and F. Bresme, Phys. Chem. Chem. Phys. **19**, 3244 (2017).
[47] R. Holyst, M. Litniewski, D. Jakubczyk, M. Zientara, and M. Wozniak, Soft Matter **9**, 7766 (2013).
[48] M. Neek-Amal, F. Peeters, I. Grigorieva, and A. Geim, ACS Nano **10**, 3685 (2016).
[49] J. Lane, M. Chandross, M. Stevens, and G. Grest, Langmuir **24**, 5209 (2008).
[50] E. Secchi, S. Marbach, A. Nigues, D. Stein, A. Siria, and L. Bocquet, Nature (London) **537**, 210 (2016).